Engineering Geology 347 (2025) 107936

Contents lists available at ScienceDirect

Engineering Geology

journal homepage: www.elsevier.com/locate/enggeo

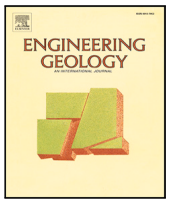

Cultural activity and impact of extreme weather events revealed by ambient seismic noise and perspective on quick clay failure monitoring in Oslo, Norway

Charlotte Bruland [a,*], Anna Maria Dichiarante [a], Andreas Köhler [a,b], Volker Oye [a,c], Ivan Van Bever [a], Eric Larose [d]

[a] NORSAR, Gunnar Randers vei 25, 2007, Kjeller, Norway
[b] Department of Geosciences, UiT - The Arctic University of Norway, N-9037, Tromsø, Norway
[c] Department of Geoscience, University of Oslo, 0371, Oslo, Norway
[d] ISTerre, CNRS, Université Grenoble Alpes, 38000, Grenoble, France

ARTICLE INFO

Dataset link: https://www.fdsn.org/networks/detail/4X_2021/, https://frost.met.no/index.html, https://sildre.nve.no/

Keywords:
Urban noise
Environmental seismology
Quick clay
Seismic interferometry

ABSTRACT

The study of urban seismic noise offers various approaches to monitor cities, from source identification to structural investigations. We demonstrate its potential to monitor cultural activity and quick clay failure in Oslo, Norway using low-cost seismic sensors. We identify train passages, a rock concert, construction blasts, local earthquakes and a meteor. To retrieve seismic velocity variations in the near subsurface, we apply seismic interferometry to three years of urban noise (1–4 Hz) recorded at four sensors, two in a quick clay risk area. Despite urban noise variability, we obtain stable noise correlation functions using 1-day-stacks. The extracted velocity variations reveal changes in the ground due to freezing and thawing as well as due to pore pressure variations related to snowmelt and rainfall. Along with anti-correlation of velocity variations and pore pressure, we observe hysteresis associated to the soil's water retention under different moisture conditions, which could provide insights into potential landslide hazard. A sharp velocity drop accompanying the heavy rainfall associated with an extreme weather event is observed. All these observations give us insights to what subsurface changes can be resolved and expected over longer time periods, which will allow us to identify unusual and permanent changes, e.g., related to quick clay. Theoretical dispersion curve analysis shows that lowering the velocity in a section of the sedimentary layer containing quick clay reduces surface wave velocities within the frequency range of interest. These results suggest that measuring velocity variations at our study site has the potential to detect quick clay instabilities.

1. Introduction

The study of urban seismic noise allows for a variety of innovative approaches to monitor cities, including cultural activities and environmental changes. Ambient seismic noise measured in urban areas contains a multitude of complex, interfering signals, which makes traditional seismological data analysis a challenging task. Still, such records include retrievable information about the sources of the ambient seismic wavefield, the subsurface structure the waves are propagating through, and the time-varying properties of sources and propagation.

For example, with seismic noise we can track population movements from cultural activities, such as concerts, football matches, fireworks and political protests (Díaz et al., 2017; Maciel et al., 2021), and identify periods of quieting, such as a result of the global COVID-19 pandemic lockdown measures (Lecocq et al., 2020) or locally, for example due to a truckers' strike in Brazil (Maciel et al., 2021). Seismic ambient vibrations can also be used to monitor road and subway traffic (Díaz et al., 2017; Riahi and Gerstoft, 2015).

Structural investigations of the urban subsurface are essential for a variety of reasons, including risk assessment related to potential natural disasters such as earthquake site effects, sinkholes and landslides, the latter including identifying areas prone to landslides and pre-cursor signals (e.g., Tomás et al. (2018), Mainsant et al. (2012), Milana et al. (2020), Le Breton et al. (2021)). In contrast to other geophysical exploration methods, such as active seismic measurements, using passive noise recordings to image the subsurface and changes therein is a cost-effective and logistically simpler approach, as it only requires deployment of a sensor network and no generation of artificial sources. Sensors can be deployed in different urban environments (e.g., in

* Corresponding author.
E-mail address: charlotte.bruland@norsar.no (C. Bruland).

https://doi.org/10.1016/j.enggeo.2025.107936
Received 18 October 2024; Received in revised form 16 December 2024; Accepted 21 January 2025
Available online 1 February 2025

buildings or parks) and can operate under various conditions (e.g., in summer or winter) (Le Breton et al., 2021). One of the most popular methods is cross-correlating continuous noise records between seismic sensor pairs or auto-correlation of noise at a single sensor, which allows creating virtual sources, a method known as passive seismic interferometry (Lobkis and Weaver, 2001; Campillo and Paul, 2003). Passive noise interferometry (or coda wave interferometry if real events are used as sources) can be applied in a time-lapse manner to retrieve temporal seismic velocity changes (Sens-Schönfelder and Wegler, 2006). This technique has various applications, from structural health monitoring (Salvermoser et al., 2015) to monitoring environmental fluctuations, such as changes in groundwater level (Lecocq et al., 2017; Fokker et al., 2021; Rodríguez Tribaldos and Ajo-Franklin, 2021), permafrost (James et al., 2019; Lindner et al., 2021; Albaric et al., 2021) and geothermal systems (Sánchez-Pastor et al., 2019). It has also been applied to investigate natural hazards, with a wide range of applications including monitoring volcanic activity (Brenguier et al., 2008; Chouet and Matoza, 2013; Schimmel et al., 2011; Masterlark et al., 2010; Duputel et al., 2009). There are also several, but fewer, studies on monitoring landslides with noise interferometry (Mainsant et al., 2012; Larose et al., 2015; Voisin et al., 2016; Bontemps et al., 2020).

In Norway, quick clay landslides are a substantial natural hazard, especially since many urban areas are located in potential quick clay hazard zones. When disturbed, the structure of quick clay can suddenly collapse, flow and behave as a liquid, potentially affecting large areas. Such quick clay slides can be triggered by overloading, erosion, heavy rainfall, snow melt, earthquake or construction work, that disturb the quick clay sediments (Khaldoun et al., 2004; Okamoto et al., 2004). Rørstadbotnen et al. (2023) investigated changes in shear wave velocity during construction work in an area with quick clay in the subsurface, in Trondheim, Norway, using early arrival direct surface waves retrieved from ambient noise cross-correlations and distributed acoustic sensing, and did not detect any subsurface change, which is expected since the quick clay did not collapse and also because direct waves are not very sensitive to tiny changes. However, applications to detect small relative velocity changes in the later arriving coda of the noise cross correlation in a quick clay area, are absent to the authors' knowledge.

The later arriving coda is more sensitive to small subsurface changes because they travel longer through the medium, and are therefore suitable for monitoring smaller relative velocity changes (Snieder et al., 2002; Obermann et al., 2016). Monitoring quick clay is becoming more important because of increasing frequency of extreme weather events, as well as new urban developments and increased pressure for building on land which has not previously been used for this purpose. In this work, we investigate the potential for monitoring subsurface changes and precursors of quick clay landslides in an urban environment in Oslo, Norway, with coda wave interferometry. We use seismic noise and low-cost seismic sensors in order to demonstrate the feasibility of using ambient noise to identify rigidity loss during, and hopefully prior to quick clay failure.

To get reliable measurements from passive seismic interferometry, we need information about the ambient noise field and how it changes over time, as well as seasonal and environmental velocity fluctuations. Therefore, we first explore the passive seismic recordings of a temporary seismic network deployed in the city of Oslo. We show the variety of seismic signals that can be detected using an urban network of low-cost seismic sensors. Second, three years of these urban seismic noise records are used to probe the subsurface in a busy, urban area susceptible to quick clay landslides. Then, the extracted velocity variations are related to environmental parameters, and the sensitivity to a velocity change at depth in the frequency range used for analysis is verified. The time period analyzed includes annual temperature variations ranging approximately from −20 °C to ca. +25 °C and extreme weather events, such as the low pressure system "Hans" in August 2023, which produced heavy rainfall with estimated 80–100 mm of precipitation within 24 h. Lastly, the potential for quick clay failure monitoring is discussed. The three years of seismic measurements represent an initial effort to establish a baseline of the seasonal and environmental velocity fluctuations in the area, which is required to be able to detect velocity variations that are permanent or out of the ordinary, and that could be related to changes in quick clay stability.

2. The Oslo seismic network

Starting in May 2021, three-component Raspberry shake sensors were deployed at different locations in Oslo (Köhler et al., 2024). The sensors were installed in basements of private businesses, houses and public schools, covering areas with construction activities such as new water supply and metro tunnel project (Fig. 1). The locations are also near critical infrastructure, such as the harbor and the cargo terminal. Additionally, the Norwegian Water Resources and Energy Directorate (NVE) has identified danger zones representing release areas for quick clay landslides based on topographical, geotechnical, and hydrological criteria. Three of these medium hazard zones are situated at or near the seismic sensors (Fig. 1a–b, https://temakart.nve.no/tema/kvikkleire). The sensor network was gradually extended, with up to 9 sensors recording simultaneously from June 2022 to July 2023. Of these sensors five are located in the Alna area (ALNN1, ALNN2, ALNN3, ALNN4 and ALNN7), three in the Linderud Area (ALNN5, ALNN6 and ALNN8) and one at Ekeberg (EKBG1) (Fig. 1a). Data are recorded continuously, with a sampling rate of 100 Hz, with the sensors having a corner frequency at about 4.5 Hz. Data are transferred in real-time. In this work, we focus on the Alna area and use data of two stations (ALNN3 and ALNN7) located in a quick clay zone. Alna is a busy urban area in Oslo, with the largest cargo terminal in Norway, a shopping center, private residences and business buildings (Fig. 1). For comparison, we also include two of the stations at Linderud (ALNN5 and ALNN6), approximately 1.3 km north of the Alna stations. We selected these stations based on the fact that they have the longest continuous records.

According to maps from the Geological Survey of Norway (NGU), both Alna and Linderud areas are underlain by sea and fjord deposits with continuous cover and bedrock consisting of Cambro-Silurian sequences which consist predominantly of shales and limestones. The sedimentary thickness map (https://geo.ngu.no/kart/losmasse_mobil/) marks both areas as covered by "sometimes very thick" sediments (see thickness map in Fig. 1). However, this map is for a regional overview purpose only, and precise bedrock depths values are not reported. Borehole data from the National database for ground surveys (NADAG, https://geo.ngu.no/kart/nadag_mobil/ and from the National groundwater database (GRANADA, https://geo.ngu.no/kart/granada_mobil/, NGU) provide more detailed information about sediment thickness at the borehole location. The closest borehole to the ALNN3 station (approximately 30 m away) indicates that the bedrock lies at 37 m depth, and that quick clay was encountered. However, bedrock depth can vary substantially over short lateral distances (Fig. 1b). The closest borehole to the ALNN5 station at Linderud is located at larger distance from the station (approximately 300 m away), but generally shallower depth are observed in this area compared to the Alna site.

The cost of a three-component Raspberry Shake seismic sensor is less than 1000 Euros. For reference, broadband seismic sensors are 10 times as expensive, while geophones plus digitizer are around 2–4 times the cost of a Raspberry Shake. Although mostly used for citizen science, Raspberry shakes have been used to quantify anthropogenic noise, for example road traffic (Healy, 2023), to show global reduction in noise levels as a result of the COVID lockdown (Lecocq et al., 2020), or to identify the signature of explosives used in a robbery (Hinzen et al., 2022). Holmgren and Werner (2021) used Raspberry shake sensors for initial examination of induced seismicity for seismic hazard purposes in Cornwall, UK. Bottelin and Baillet (2024) used modal frequency to track rock column pre-failure with Raspberry shakes. Köhler

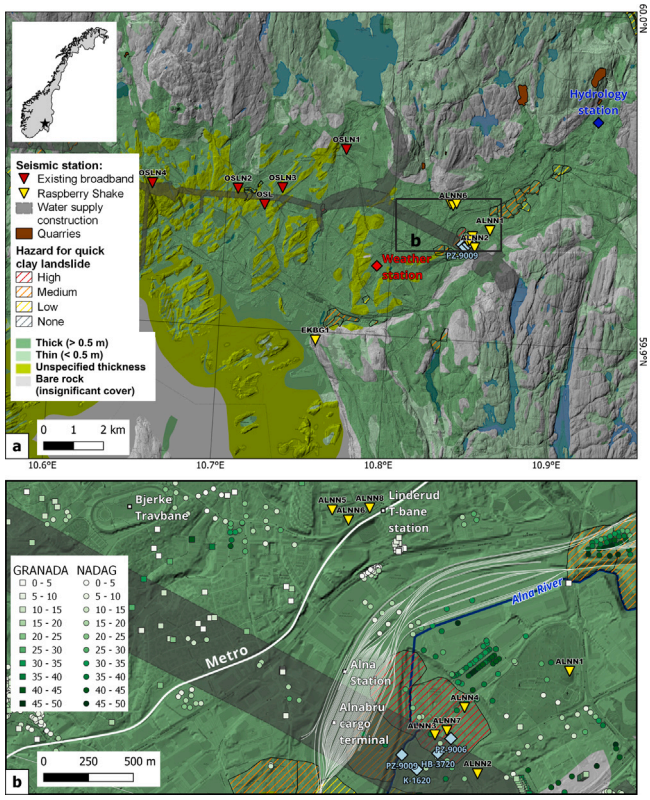

Fig. 1. Overview maps of the study area: (a) Bedrock thickness map provided by the Geological Survey of Norway (NGU) draped on the 10 m resolution DEM (shaded relief) by the Norwegian Mapping Authority (https://hoydedata.no/LaserInnsyn2/). Seismic stations deployed during this study are shown in yellow, while existing broadband stations in red. Quick clay hazard areas mapped by the Norwegian Water Resources and Energy Directorate (NVE), quarries and relevant infrastructures are also shown. The location of the weather and hydrology stations are shown by a red and blue diamond, respectively. (b) Close up of the study area in a showing also the location of the Alnabru cargo terminal, the metro, the Alna and Linderud stations, and the Bjerke Travbane. The Alna river and the piezometers in the Alna region are shown as light blue diamonds. Boreholes from the GRANADA and NADAG databases are shown color-coded by depth to bedrock (https://geo.ngu.no/kart/nadag_mobil/ and https://geo.ngu.no/kart/granada_mobil/, respectively). (For interpretation of the references to color in this figure legend, the reader is referred to the web version of this article.)

et al. (2024) used the seismic network of the current study to investigate a multitude of construction and quarry blasts in the city Oslo. Raspberry shakes have also been used for noise-based subsurface investigations. Ghione et al. (2023) utilized the Horizontal to Vertical Spectral Ratio (HVSR) from Raspberry Shake recordings in conjunction with a statistical geological mapping tool (COHIBA) to estimate both the depth to bedrock and the local average shear wave velocity in the uppermost 30 meters of the ground (Vs30). The Vs30 parameter is commonly employed in seismic hazard assessments to classify soil types and determine soil amplification. There are very few studies on the potential for ambient noise interferometry using Raspberry shakes, but the potential for passive shallow applications were demonstrated by Arosio et al. (2023).

3. Ambient seismic noise levels

Seismic noise levels at different locations allow us to characterize the seismic signature of an urban environment. We begin with analyzing changing noise levels over time. To evaluate the noise level at the different locations in Oslo, we use the probabilistic power spectral density (McNamara and Buland, 2004) of the noise amplitude records, which is compared to global reference models for seismic noise, the New High- and New Low Noise model (Peterson et al., 1993). The models are constructed from the envelopes of a large number of vertical seismic records from globally distributed stations, so the low- and high noise models would correspond to the most quiet and noisy locations on Earth, respectively. Noise levels for eight different stations of the Oslo seismic network are shown in Fig. 2.

All stations display high noise levels, where the majority of the power spectral densities are close to or even above the New High Noise model. This is characteristic for urban seismic records. Still, the noise levels vary across the network, especially for higher frequencies, with the highest noise levels observed at Alna (ALNN3, ALNN4 and ALNN7). Lower noise levels are observed at Linderud (ALNN5 and ALNN6) and Ekeberg (EKBG1). About 70% of all cargo traffic by trains in Norway passes through the cargo terminal at Alna, and trucks deliver and collect cargo containers almost around the clock, which explains the higher noise levels. The heavy road traffic in the area due to the presence of many private businesses, shopping malls, and private residences, contribute to the high noise levels, which provide the potential to utilize frequencies below the natural frequency of the instrument.

Above 1 Hz, seismic noise in urban areas is dominated by anthropogenic sources (Groos and Ritter, 2009), such as car and train traffic. Furthermore, we expect significant temporal variation between day and night as well as weekdays and weekend due to regular patterns in human rhythm of life. These two regimes (lower and higher noise levels) are visible as two curved areas with high counts for all stations in Fig. 2. The temporal variation of the power spectral density for two different locations for ALNN6 and ALNN7 at 2 Hz is shown in Fig. 2, also clearly revealing the diurnal and weekly variations. ALNN6 is placed in the basement of a public school at Linderud. Hence, in addition, we clearly see the influence of school holidays, with lower noise levels for both the longer summer holidays in June, July and August, as well as shorter holidays, such as Easter, following the opening hours of the school. This is not the case for the stations located close to the cargo terminal, where activity is constantly high (Fig. 2). The urban rhythm may limit the applicability for seismic interferometry due to noise source variability affecting the velocity change measurements, but the consistently high noise levels at Alna can also be beneficial for noise-based monitoring.

4. Specific noise sources

After obtaining an overview about temporal and spatial variability of noise levels, we can search for specific anthropogenic events in this seismic signature of the city of Oslo.

4.1. Concert

Music festivals and concerts are known to generate vibrations that can be recorded by seismic sensors (Erlingsson and Bodare, 1996; Denton, 2014; Díaz et al., 2017; Tepp et al., 2024). These signals typically exhibit narrow, harmonic frequency peaks between 1 and 10 Hz that last for minutes, resembling harmonic tremor observed at active volcanoes. On the 24th July 2022, 60 000 spectators witnessed a concert of the heavy-metal band Rammstein at about 1.5 km (see Bjerke Travbane in Fig. 1b) from one of the sensors at Linderud (ALNN6 in Fig. 1b). Signals originating from the concert were recorded at all seismic sensors in that area. Fig. 3 shows the vibrations from the concert recorded at ALNN6.

Looking into the frequency content of the recorded signal over time, distinct spectral peaks can be observed between around 2 to 5 Hz. The fundamental resonance frequency for this station is between 4–6 Hz, which could explain why the harmonics in this frequency range are the strongest. The different songs from the set list of the concert can be identified in the spectrogram, with the frequency peaks corresponding to the tempo of the different songs. To obtain the tempo (beats per minute, BPM) of each song, we conducted an online search using publicly available data. The pianist's opening for Rammstein and the

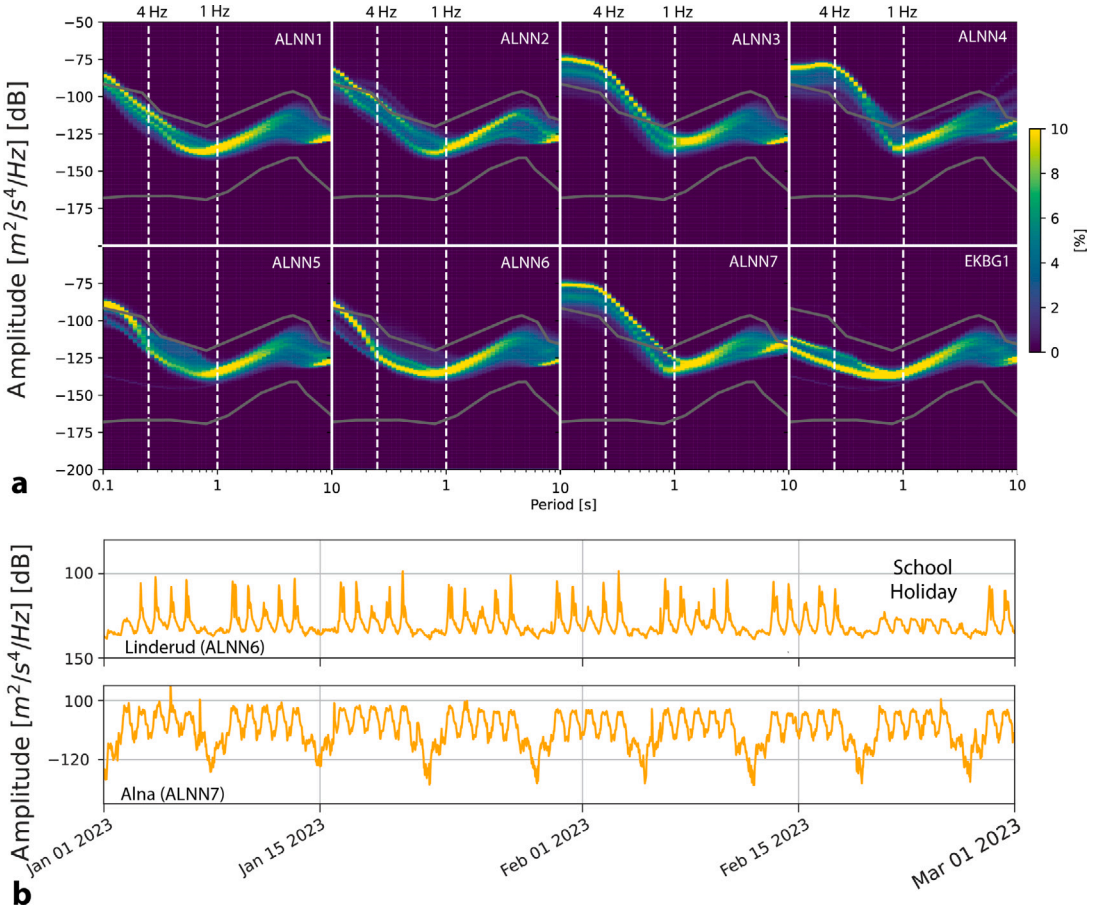

Fig. 2. Noise levels at 8 different stations in the Oslo network: The probability power spectral density is calculated for hourly power spectral densities with an overlap of 50 % for all available data from 2021 to 2023. The color scale shows the percentage of the spectra at a given period and amplitude, while the solid lines represent the New High and Low Noise models (Peterson et al., 1993). The dashed vertical lines point to the frequency range (1–4 Hz) that is used for the correlation analysis (see Section 4). The temporal evolution of the power spectral density at 2 Hz for ALNN6 (Linderud) and ALNN7 (Alna) is shown in (b). (For interpretation of the references to color in this figure legend, the reader is referred to the web version of this article.)

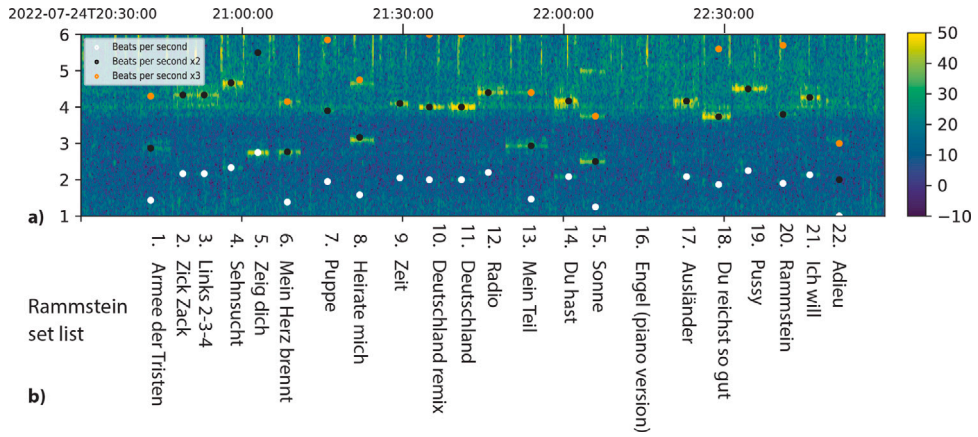

Fig. 3. Seismic signature of Rammstein: Vibrations from the Rammstein concert on the 24th of July 2022 detected at Linderud: (a) shows the signal in time on the vertical component, bandpass filtered between 1 and 6 Hz, while (b) displays the spectrogram of the signal calculated with a 30 s window length and 50 % overlap. The different songs are identified from the seismic records and the tempo (beats per second), fundamental frequency and first two harmonics, for the different songs are superposed on top of the same spectrogram in (c) for the set list shown in (d). (For interpretation of the references to color in this figure legend, the reader is referred to the web version of this article.)

piano version of the Rammstein song "Engel" are not visible in our seismic noise records.

Different mechanisms have been proposed to generate concert trem ors, such as the crowd moving to the beat or vibrations from the sound system. Both mechanisms can be explained through the Dirac comb effect (the Fourier transform of an evenly spaced series of spikes is a series of spikes, with frequency spacing between the spikes equal to the inverse of the period between the spikes in time). The vibrations observed at Linderud are likely attributed to a combination of the crowd moving to the beat of the music and the sound system.

4.2. Metro traffic

The seismic station recording the concert is located close to the metro station at Linderud (ALNN6, Fig. 1b). The trains passing the station are observed in the spectrogram as vertical lines starting at around 5 Hz (Fig. 3). Train passages typically generate tremor-like broadband emergent signals with harmonic spectra with frequencies between 2–40 Hz (Fuchs et al., 2018).

For the three stations located close to the Linderud metro station (ALNN5, ALNN6 and ALNN8), these train signals are dominating the passive records for frequencies above 5 Hz. In Fig. 4, we show the detection of westbound and eastbound trains, appearing in time-frequency as equidistant spectral lines. As the trains approach Linderud station and slow down to stop, the frequency of the signals decreases as the trains decelerate. Increasing frequencies are observed when the trains start to move again and accelerate when leaving the station. Several studies have aimed on characterizing train induced vibrations to understand the physical mechanisms behind the observed signals (Riahi and Gerstoft, 2015; Fuchs et al., 2018; Lavoué et al., 2021). Lavoué et al. (2021) showed that the spectra of the signals originating from trains are modulated by the distance between the wheels, with frequency content controlled by the distribution of axle loads over the rail, which largely depends on ground stiffness below the railway. Localized noise sources can cause problems for seismic interferometry, but also has potential as an opportune source for imaging and monitoring the subsurface.

4.3. Blasts, earthquakes and meteors

While metro signals can only be recorded on close sensors (50 to 180 meters from the station), and concerts are relatively rare events, blasts generate signals which can be observed at larger distances, across the whole network, and are frequent in Oslo. Köhler et al. (2024) analyzed the data of the same network used in this study to detect construction and quarry blast in and around the city of Oslo. Between 2021 and 2023, over 1,200 blast signals from several distinct locations have been identified with up to 10 events each day. The prominent signal observed throughout the entire network was the surface wave (0.8–2 Hz). The blasts originate mainly from metro and water tunnel constructions in Oslo. These infrastructure upgrades are necessary due to the continuous population growth in Oslo. Monitoring blasts in (growing) urban areas is beneficial for example to detect unusually large events where the ground motion may lead to structural damage or simply alerts citizens when they experience shaking. More details and examples of blast signals can be found in Köhler et al. (2024).

We also detect natural events, such as earthquakes. Figure A.11 shows signals from two earthquakes, happening 5 min apart, just across the Swedish border at approximately 120 km southeast of Oslo with magnitudes 2.8 and 2.2, as well as a 5.1 magnitude earthquake in the North sea on the 21st March 2022 (Jerkins et al., 2024). Acoustics signals coupling with the ground from a meteor passing over Oslo on the 24th of July 2021 were also detected on the seismic sensors.

5. Measuring relative velocity changes from passive noise recordings

As shown in the previous section, ambient noise contains an abundance of hidden signals. Despite the high noise levels, we are able to identify train passages, a rock concert, construction blasts, local earthquakes and a meteor and, undoubtedly, many more signals could be retrieved from this rich record. These examples highlight the potential for urban monitoring, as already suggested by previous studies. Potential applications based on these findings include, but are not limited to monitoring traffic, trains and explosions. However, our focus up to this point has been on identifying sources and we have not yet explored using the recorded noise for structural investigations, which may prove to be the most powerful application of urban seismic networks.

A decrease in seismic velocity can be a landslide precursor several days or hours before failure since it is a direct indication of softening of the underground layers (Larose et al., 2015; Le Breton et al., 2021). From seismic noise, we can measure the relative change in seismic velocity (dv/v) which allows us to potentially identify these precursors. However, a careful analysis has to be conducted to identify such precursors, since fluctuations in velocity are also caused by a number of other factors including noise field variations (source variability) or other environmental changes not being the monitoring target.

5.1. Data processing

We apply passive seismic interferometry (Sens-Schönfelder and Wegler, 2006) to three years of urban seismic noise records of four stations in the Oslo network, two located at Linderud (ALNN5 and ALNN6), close to a metro station, and two stations at Alna (ALNN3 and ALNN7), in a quick clay zone close to the cargo terminal (see Fig. 1). In passive seismic interferometry, empirical Green's functions (EGFs) are first estimated using cross-correlation of seismic noise for short time windows. Second, the short-term noise correlations are compared to a long-term reference. The relative changes in elastic and structural properties of the medium are measured through subtle dilations and distortions in the coda of the EGF waveforms using the stretching method. The EGF coda is used instead of the direct (ballistic) arrivals since it is more sensitive to changes in the medium and less affected by noise source variability.

In our case, both autocorrelations and single station cross-correlat ions between vertical and horizontal components are computed using the Seismic software (Makus and Sens-Schönfelder, 2023). Before computing the correlations, the data is pre-processed in daily segments. The same processing is applied to all sensors and component combinations. First, the data is downsampled to 25 Hz, then detrended, tapered and bandpass filtered in three bands: 1–2.5 Hz, 1.5–3 Hz and 2–4 Hz. We focus on high frequencies (between 1–4 Hz) as instrument noise dominates below 1 Hz (Ghione et al., 2023), and the sensitivity of seismic velocities to the near surface structure, where quick clay is typically located, is high in this frequency band. To exclude earthquakes and other transient events, amplitudes higher than 2.5 times the standard deviation are clipped. We slice the data into 1-hour-long windows and compute correlation functions in the Fourier domain.

Passive seismic interferometry is based on the assumption that the sensors are evenly surrounded by uncorrelated noise sources, and/or stacking long enough time series for the correlations to converge to the EGF. However, Hadziioannou et al. (2009) showed that these requirements can be relaxed for monitoring purposes. Still, stable background noise sources, in time and space, is important for stability of noise correlation functions. We stack the hourly noise correlations to average the changes in noise sources. In general, the more time we stack, the more stable noise correlation functions we get. Since we know that noise is strongly affected by the urban rhythm, we use both a 1-day stack, to average the day-night time noise variation, for

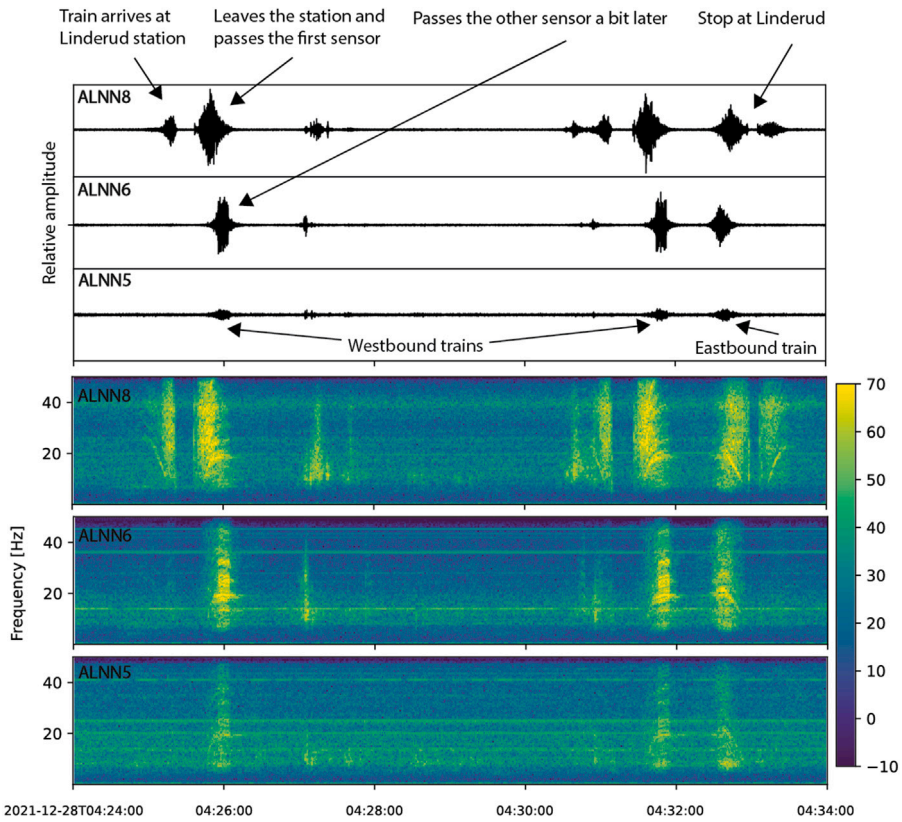

Fig. 4. Seismic signature of trains at the Linderud train station: (a) Seismograms showing 10 minutes of vertical component passive recordings at % Linderud (ALNN8, ALNN5 and ALNN6). (b) Spectrogram from the same stations calculated with 3 second windows and 90 % overlap. (For interpretation of the references to color in this figure legend, the reader is referred to the web version of this article.)

higher temporal resolution needed for monitoring, and a 7-day stack to average the weekday-weekend noise variation for comparison. To get "daily" resolution for the relative velocity change (dv/v) in the case if the 7-day-stack, we slide one day forward and then stack the hourly correlations over the 7 previous days to obtain the next data point in the dv/v time series.

The resulting daily correlation waveforms for the vertical component autocorrelations over time from 2021-05-19 to 2024-07-26 for stations ALNN3 and ALNN7 at Alna filtered between 1–2.5 Hz are shown in Figure A.12. Since the autocorrelation is symmetric, we only show one side. We have stable coda wave arrivals for both stations up to 20 s. We see a clear shift in the arrivals in the coda, with earlier arrivals, i.e., higher velocities during winter months, dominating the temporal variation of the noise correlation functions. Before measuring the time shift from the 1-day- and 7-day-stacks, the correlations are again filtered in the three target frequency bands: 1–2.5 Hz, 1.5–3 Hz and 2–4 Hz.

By measuring the relative time-shift between the noise correlation waveforms, we can retrieve the relative change in seismic velocity (dv/v) (Snieder et al., 2002). Here, we use the trace stretching technique (Sens-Schönfelder and Wegler, 2006), but there are also other methods that can be used to estimate the seismic phase delays (Mikesell et al., 2015). The average of the correlations for the whole time period is used as a reference for the stretching. For coda windows between 2 and 15 s (shown in Figure A.12), we carry out a grid search over different stretching factors between −0.1 to 0.1 with an increment of 0.0001, to allow for the large velocity variations. We use the early coda and broader, overlapping frequency bands to minimize cycle skipping due to large velocity fluctuations. The best match is the stretching factor with the highest correlation coefficient and provides the estimate for the relative velocity change. We carry out the stretching separately for the causal and acausal side of the correlation waveform and average the obtained stretching factors. Since the coda is composed of scattered waves, it samples the medium multiple times and has a longer propagation path in the medium. Therefore, the method is sensitive to small changes in the medium and to a larger area.

For each component combination (ZZ, ZN, ZE, EE, EN and NN), we obtain a similarity matrix which contains the results from the trace stretching, i.e., the correlation coefficient between the stretched trace and the reference for the different stretching factors tested for all time steps (daily) of the time period analyzed. We then compute the station averaged velocity change by averaging the similarity matrices of the different component combinations we want to use (can also be just a single one). The station averaged dv/v then corresponds to the stretching factor with the highest cumulative correlation coefficient of the averaged stretching matrices (Illien et al., 2023; Makus et al., 2023).

5.2. Observed velocity variations due to environmental changes

We first consider the seismic velocity changes retrieved from vertical component autocorrelations. From previous landslide studies, we know that environmental influences can cause seasonal seismic velocity changes, which can vary from 1 to 6% (Le Breton et al., 2021). To distinguish velocity changes that could be related to potential instabilities in quick clay, we need to identify the seasonal, environmental fluctuations. Temperature, water content, snow depths and air pressure can affect seismic velocities in the subsurface. Often, these effects interfere, making it difficult to differentiate between them. In an attempt to understand the seismic velocity fluctuations in terms of subsurface changes, we relate the daily velocity changes to measurements of air temperature, precipitation, water level in a nearby river, and pore pressure in a well nearby. An overview of these environmental data compared to the dv/v at ALNN3 is shown in Figure A.13. The time period investigated includes a very dry summer in 2022, the extreme

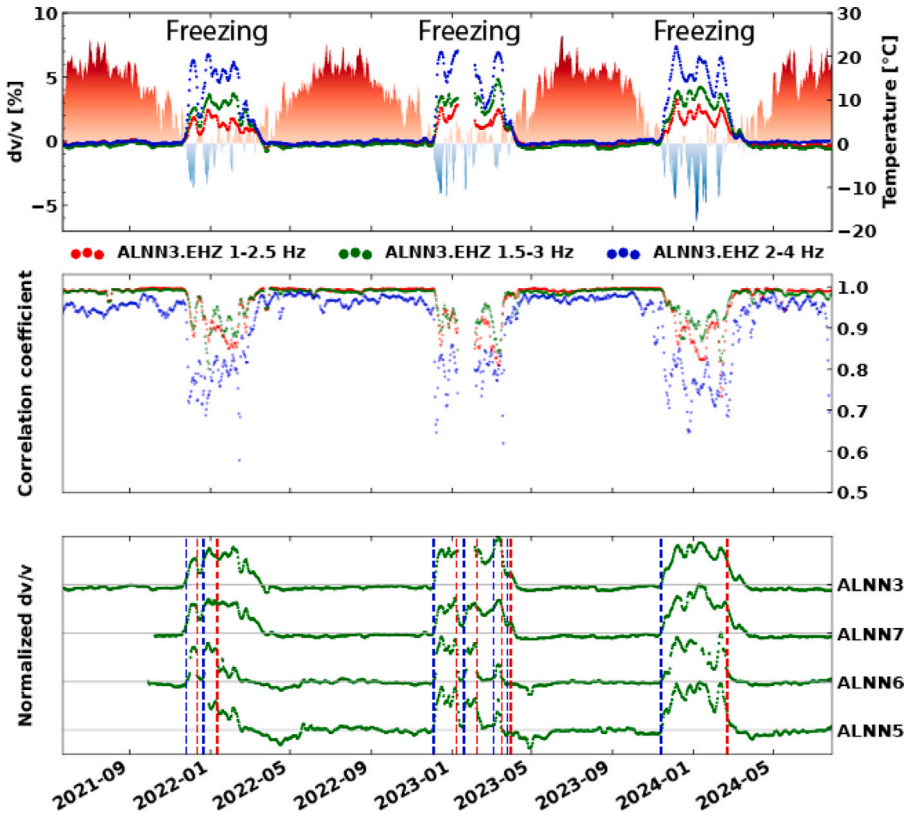

Fig. 5. Freezing and thawing: Relative changes in seismic velocities over three years calculated for three different frequency bands is displayed in the top panel, superposed on the air temperature measured. The middle panel shows the correlation coefficient from the associated stretching factors displayed in the top panel for the same frequency bands. In the bottom panel, the normalized dv/v for the four seismic stations is shown. Vertical lines are interpreted as freezing (blue) and thawing (red) from when the temperatures stay below or above zero degrees for 5 consecutive days. (For interpretation of the references to color in this figure legend, the reader is referred to the web version of this article.)

weather "Hans" in 2023, the very cold winter of 2023/2024 and a very wet summer in 2024. First, we try to entangle the effect of freezing and thawing on the near subsurface velocities.

5.2.1. Freezing and thawing

As the temperature decreases below zero and the soil gradually starts freezing, it becomes more rigid and the seismic waves travel faster. Therefore, we can use coda wave interferometry to track freezing and thawing cycles (James et al., 2019; Albaric et al., 2021). Steinmann et al. (2021) showed that a frozen layer of less than 5 cm can cause apparent velocity increases above 2%, depending on the components used for analysis, since Rayleigh and Love waves have different sensitivity to superficial freezing.

Fig. 5 shows the extracted relative changes in seismic velocity and the highest correlation coefficient from the stretching in different frequency bands for station ALNN3 at Alna together with the air temperature, as well as a comparison for ALNN3, ALNN7, ALNN5 and ALNN6, in the frequency band 1.5–3 Hz. The latter frequency band provided stable results for all four stations. We use the 7-day-stack when comparing different frequency bands and stations to account for the different variations in noise sources. The strong increase in apparent velocities during the winter months, that we already observed in the correlation waveforms (Figure A.12), is very well anti-correlated with temperature. The freezing effect is visible in all frequency bands and stations used for analysis. For ALNN3, we observe a clear trend with stronger velocity changes for higher frequencies, with an increase of 2 % and 7 % for the highest frequencies used for analysis (Fig. 5). The increase in seismic velocity is also accompanied by a decrease in correlation coefficient obtained from the stretching. The decorrelation increases with increasing frequencies.

The winters over the time period analyzed become increasingly colder, both in terms of temperature and duration of freezing periods. The winter in 2022 and 2023 show a similar pattern with the coldest temperatures recorded in the beginning of the season (~ 15 January), while the winter 2024 has an early onset with temperature below zero registered already in mid November, but the lowest recorded temperature is registered in January.

Of the four stations we describe above, two are located in the mapped quick clay hazard area at Alna (ALNN3 and ALNN7) and two outside that area at Linderud (ALNN5 and ALNN6). At Alna, thick sediments (ca. 37 m) have been intercepted at the closest borehole and quick clay mapped within the shallower 30 m. The presence of ca. 1 m of fill material at the very top of the borehole is also documented. No similar information is available for Linderud but we can expect thinner sediment (ca. 10 m) over the bedrock (ALNN5 and ALNN6). We observe the impact of frozen ground at both location, with the freezing occurring simultaneously at all stations. However, thawing begins earlier at the Linderud stations. Given the recorded air temperature, the maximum depth of the active thermal layer at both locations has a maximum thickness of 1 m. Therefore, the difference in thawing behavior may be linked to variations in shallow (less than 4 m) soil composition, which affects how water and heat are retained, as well as differences in ground vegetation, which influence sunlight absorption. Additionally, snow cover, potentially impacted by human activities such as snow removal, could play a role. However, it is so far not possible to conclusively determine the underlying cause of the observed differences related to thawing.

5.2.2. Soil moisture and groundwater levels

As the surface ice and snow melt and the ground thaws, we observe a decrease in seismic velocities. Changes in the water content affect loading and pore pressure in the subsurface. With more water in the ground, the pore pressure increases and with an increase in pore

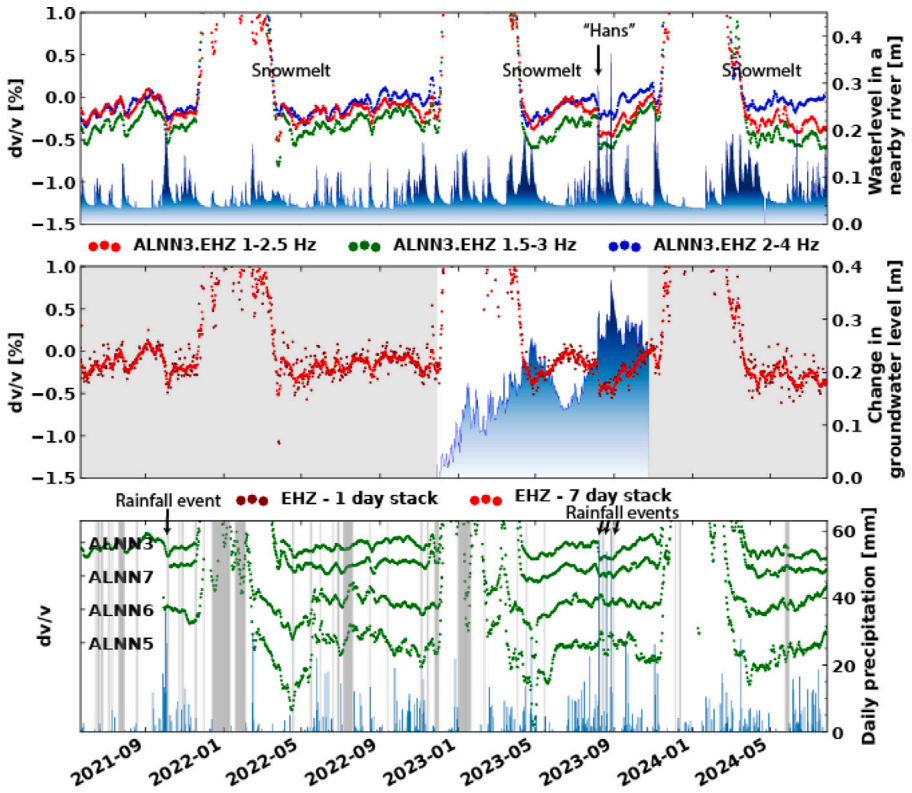

Fig. 6. Dv/v and water measurements: The top panel shows dv/v for station ALNN3 in three different frequency bands: 1–2.5 Hz (red), 1.5–3 Hz (green), 2–4 Hz (blue), using a 7 day stack, together with the water level in the Alna River, which flows through the quick clay risk area. The middle panel shows change in water level for PZ-9006 and dv/v with two different temporal resolutions, 1-day-stack in dark red and 7-day-stack in red, for 1–2.5 Hz. The bottom panel shows the dv/v for the four different stations for 1.5–3 Hz superposed on the daily precipitation. The gray shaded areas are gaps in the data. The station location and position of the river is marked in Fig. 1. (For interpretation of the references to color in this figure legend, the reader is referred to the web version of this article.)

pressure, the difference between the confining pressure and pore pressure (i.e., effective pressure) is decreasing, which reduces the seismic velocity. Therefore, seismic velocity variations can be used to track changes in pore pressure or groundwater table levels. Different studies have linked changes in seismic velocities to changes in pore pressure or groundwater levels (Sens-Schönfelder and Wegler, 2006; Clements and Denolle, 2018; Voisin et al., 2017; Fokker et al., 2023).

We compare the precipitation and changes in groundwater level to the measured changes in seismic velocity, alongside water level data from the nearby Alna river in Fig. 6, 1. The water level is derived from the pore pressure measurements from a piezometric well (PZ-9006 in Fig. 1) nearby. Pore pressure measurements from the area are shown in Figure A.14 for the wells (PZ-9006, PZ-9009, HB-3720 and K-162) shown in Fig. 1. The water level in the river is included to complement and fill gaps in the well datasets. A gradual decrease in seismic velocities, that takes longer than the thawing of the frozen ground, associated with the influx of meltwater during spring, is observed on all stations used for noise interferometry. At the Alna stations (ALNN3 and ALNN7), we observe this effect for all analyzed years when higher water levels in the Alna river are measured, which further suggests that the increase in meltwater is responsible for the velocity decrease. The changes in seismic velocity for the stations at Linderud (ALNN5 and ALNN6) are sharper, more rapid and larger in magnitude. This difference could be due the difference in the depth of the bedrock at the two sites (shallower at Linderud compared to Alna), which leads to different time that will take to the sedimentary layer to get fully saturated, and to the different porosity and permeability of both clay and bedrock.

Some of the drops in seismic velocity also coincide with precipitation and an increase in water level in the Alna river (Figure A.13). For example, there was one large rainfall event later in fall 2021, however, only one station (ALNN3) was recording at the time. Here, we can also see a clear decrease in dv/v (−0.5%, depending on the frequency band). The extreme weather event “Hans” in Southern Norway in August 2023 was associated with three heavy rainfall events in the Oslo region: on the 8th, 20th and 27th of August. The precipitation on the 8th of August lead to flooding that affected the power supply at ALNN3. This resulted in a gap of about 20 h in the data at the start of the weather event, which causes the artifacts that we see at the start of the extreme weather (Figure A.13).

Still, we see a sharp drop in seismic velocity accompanying the heavy rainfall associated with the beginning of “Hans” (Fig. 6). The dv/v stays low for the duration of the three rainfall associated with “Hans”. The dv/v for 2–4 Hz starts decreasing earlier than for the lower frequencies, which means infiltration from the surface downwards, and returns to the same level as before “Hans” faster than the other frequency bands. This is most likely because the higher frequencies are more sensitive to the shallow changes in soil moisture, rather than being sensitive to changes in (deeper) groundwater level.

At ALNN3, for the lowest frequencies used for analysis, the dv/v is lower for “Hans” than for the snowmelt in the spring, and also the previously mentioned rainfall event during fall 2021. We see a similar pattern for the other station in the quick clay area (ALNN7) with a sharp drop in velocity, however, the dv/v is not lower for “Hans” than for the spring.

For the two stations at Linderud, we do not see a clear change in seismic velocity with rainfall, even for the extreme weather event. This could be attributed to direct runoff at the surface, due to difference in the shallow subsurface at the two sites. It could also be because the noise correlation functions are not stable enough to retrieve seismic velocity variations, and the smaller changes are masked by the variation in noise sources. In Section 5.3, we attempt to increase the stability of the measurements.

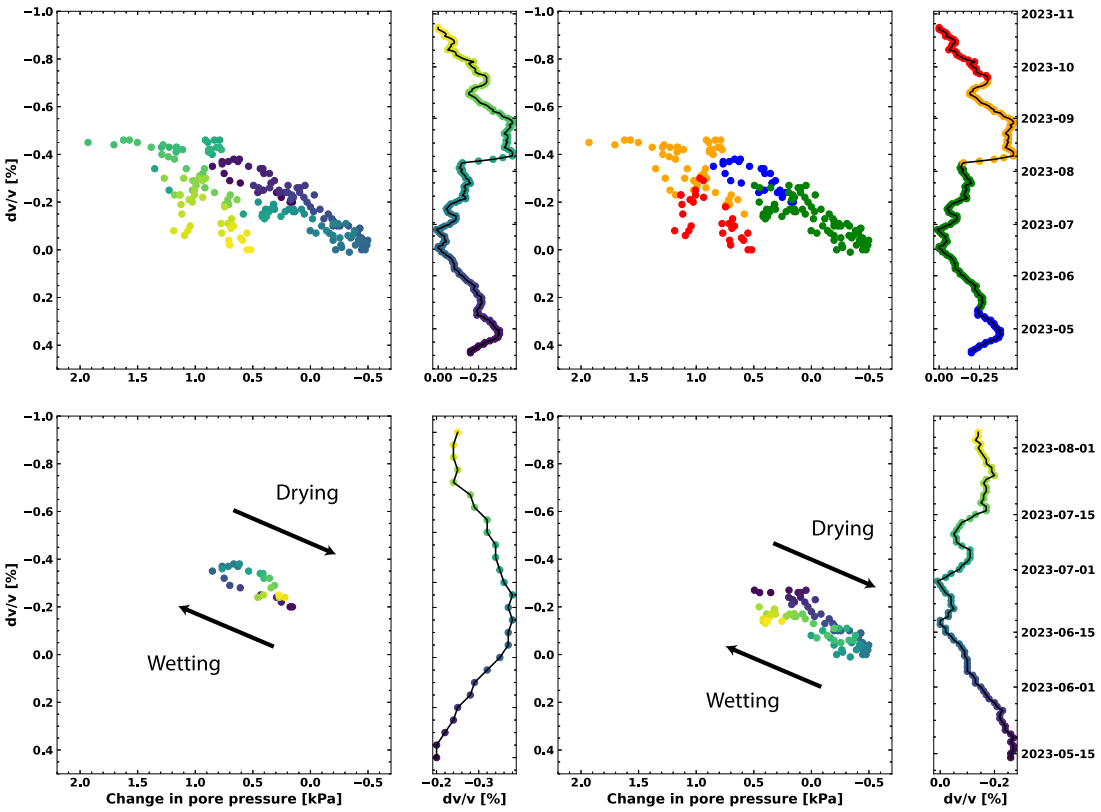

Fig. 7. Dv/v vs. pore pressure: The extracted relative velocity changes are plotted against changes in pore pressure, with (top) colors representing different time-periods. The first (blue) identified in the right top panel shows the increase in water content during snowmelt, followed by a drying period. A close-up is shown in the bottom left panel. The second period (green) is shown as close-up in the bottom right panel, and represents the subsurface drying process followed by wetting period due to rainfall. (For interpretation of the references to color in this figure legend, the reader is referred to the web version of this article.)

We see an anti-correlation between the change in seismic velocity and the groundwater level. The best correlation between the dv/v and groundwater level, we obtain for the lowest frequency band used in the study for ALNN3. Using a 7-day stack and only the time period when the ground is unfrozen, the dv/v and the groundwater level has a Pearson correlation coefficient, *r*, of −0.69, pointing towards a linear relation between the two variables. Typically, *r* larger than +/-0.7 is considered a strong linear relationship. For the 1.5–3 Hz and 2–4 Hz band, *r* equals −0.32 and −0.07, respectively. The lower the frequency, the deeper the sensitivity of the seismic waves. Hence, higher correlation at lower frequencies suggest that dv/v seems to be most sensitive to changes in the (deeper) groundwater level, rather than water content near the surface which dissipates quickly into deeper layers. Higher pore pressure is associated with snow melt and many rainfall events. However, the highest pore pressure/groundwater levels observed, follows the extreme weather "Hans" in August 2023. This is also observed in the dv/v. For the summer of 2024, the velocities are overall lower than for the previous years, and stay low, especially for the lower frequency bands used for analysis. Although we do not have pore pressure data for this time period, it suggests that the groundwater level is higher throughout this summer compared to the previous years.

A linear relation between water level and dv/v has previously been observed (Clements and Denolle, 2018; Wang et al., 2017). However, a close analysis of our observations reveals two distinct paths when plotting dv/v against pore pressure change: (i) the wetting curve, which shows how the soil retains water as it gets progressively wetter during infiltration, and (ii) the drying curve, which shows how the soil releases water as it dries. This hysteresis effect, previously been observed by Garambois et al. (2019), Gaubert-Bastide et al. (2022) in a different setting and at larger scale, shows that under typical conditions, the drying curve lies above the wetting curve. For a given suction (capillary pressure), drying soil retains more water than wetting soil. This behavior is attributed to differences in pore structure and surface tension effects during wetting and drying cycles. We can therefore use the observed hysteresis as an additional observation to better understand the soil characteristics and its behavior under changes in moisture condition. The negative pore pressure values also point towards the soil being unsaturated. (See Fig. 7).

5.3. Including horizontal components to increase stability and improve temporal resolution of noise correlations

Up to this point, we have only looked at results from vertical component auto-correlations. Often, the horizontal components are discarded due to lower signal-to-noise ratio of the EGFs. Here we investigate whether considering all components and combinations, as well as averaging different component combinations (Illien et al., 2023), can increase the stability of our measurements and in turn improve the temporal resolution of our dv/v measurements.

Typically, 1-day-stacks, meaning one day resolution, is used for monitoring natural hazards using seismic noise interferometry. In our investigation, we aim for the same. The changes in seismic velocities retrieved from different component combinations are shown in Figure A.15 and A.16 for Alna and Linderud, respectively. In general, averaging makes the dv/v curves smoother and can remove artifacts in the velocity changes for example due to noise source variations.

Apparent changes in seismic velocity can be caused by changes in the noise sources. Because our stations are placed in an urban environment and we are using high frequencies, our changes in noise sources are correlated with the pattern in the anthropogenic activity (see Section 3). Due to the week-weekend variations in the noise field, weekly fluctuations are visible in the dv/v, especially for the 2–4 Hz

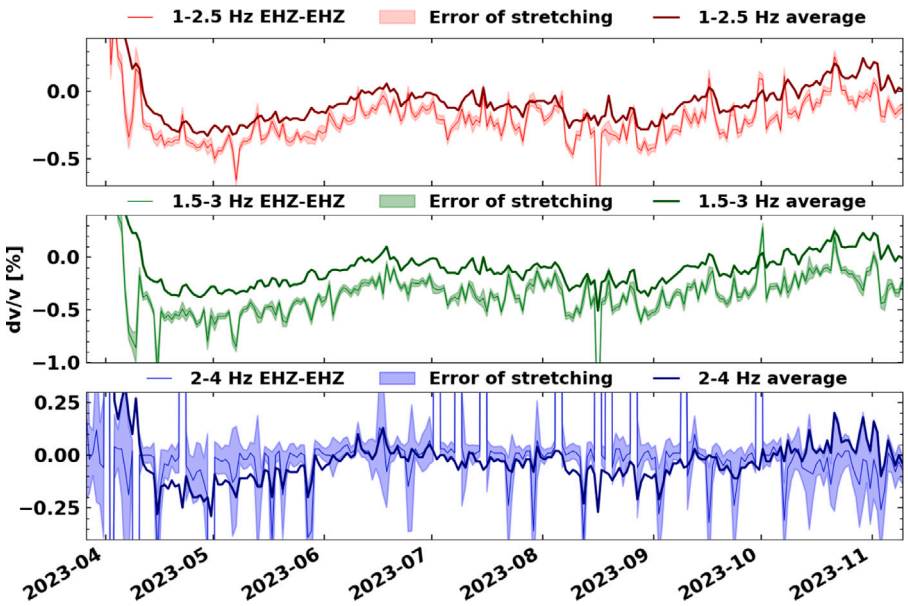

Fig. 8. Effect of averaging over different component combinations at ALNN7: The dv/v for vertical component autocorrelation and for averaging over different component combinations for a 1-day-stack is shown for three frequency bands, 1–2.5 Hz, 1.5–3 Hz and 2–4 Hz, starting with the lowest frequency band in the top panel. The shaded area represents the rms error for the stretching results (Weaver et al., 2011) of the vertical component autocorrelation. The averaging reveals a similar trend for the 2–4 Hz band as for the lower frequency bands with lower velocities in the spring and for the extreme weather event, that was previously not visible only using the vertical component. (For interpretation of the references to color in this figure legend, the reader is referred to the web version of this article.)

band (Fig. 8 and A.17 in the supplementary material). Averaging the results from the stretching helps smooth out these weekly variations and can reveal environmental fluctuations that were previously not visible using vertical components only (Fig. 8).

The early part of the coda of the noise correlation functions is dominated by surface waves (Obermann et al., 2013). In the case of the vertical component autocorrelation, only Rayleigh waves are observed, since Love wave ground motion has only horizontal components, whereas all other component combinations involve a mix of Rayleigh and Love waves. Since effects of Rayleigh and Love waves are averaged, the component averaging can cause issues by removing or dampening sudden, real changes, such as extreme weather events (Figure A.17) or sharp seasonal variations (Figure A.18).

During the freezing period, we observe different, non-consistent dv/v variations for different component combinations (Figure A.15 and A.16). This could be attributed to Love waves and Rayleigh waves responding differently to the frozen layer (Steinmann et al., 2021), cycle skipping when comparing EGFs during stretching due to large velocity changes (dv/v is underestimated), less stable correlations for some component combinations, or the changing location of the noise sources. Therefore, averaging the similarity matrix does not remove the cycle skipping effects during the winter months. Nevertheless, although averaging all component combinations does not systematically improve results, certain combinations which include horizontal components can provide high correlation coefficient and less cycle skipping in specific frequency bands. Therefore, the choice of individual combinations, including horizontal components and averaging will depend on the focus of our analysis and the stations and frequency bands used for analysis.

When not averaging, dv/v is still more sensitive to changes in noise sources. For example when only using vertical component autocorrelation at ALNN5 at Linderud (Figure A.18), specific events on the noise correlation functions in addition to the weekly variations become evident, such as the spike on 1st of May, which is a national holiday, as well as the Rammstein concert on the 24th of July (see Section 3). Seismic noise on these days was most likely originated from a dominant direction, biasing the interferometry results.

In general, the larger noise field variation at Linderud lead to less favorable conditions for seismic interferometry because of the stronger weekly variations in dv/v. On the other hand, the more constant anthropogenic activity at Alna provides favorable conditions for seismic interferometry. Despite these differences, dv/v variations caused by changes in the urban noise should be taken into consideration when interpreting the results. However, these changes that are traceable back to changes in the noise sources are significantly smaller than those attributed to environmental velocity fluctuations in the subsurface.

6. Depth sensitivity

For computing dv/v with the stretching method, we used the early coda, which is typically dominated by surface waves. The sensitivity to surface waves decreases rapidly with depth. For depths larger than 2/3 of the wavelength, the surface waves are generally much less sensitive to the structure (Obermann et al., 2013). To assess whether the frequencies used in our analysis are sensitive to change at the depths where quick clay could destabilize and initiate a landslide, we computed the theoretical Rayleigh wave dispersion curves using the Geopsy software (Wathelet et al., 2020) and HVInv software (García-Jerez et al., 2016). We inverted the measured horizontal to vertical spectral ratio (H/V) data from ALNN3 to derive a representative (best-fitting) 1D-velocity for this site (Fig. 9a and b).

To test the sensitivity, we introduced two cases, a and b, by reducing the Vs velocity of the best-fitting model by 10% and 40%, respectively, for a 5 m thick layer at 5 m depth. The dispersion curves show a decrease in surface wave velocity within the frequency range of interest, with the largest changes in the highest frequency band (Fig. 9c). For the center frequency of the different frequency bands (1–2.5 Hz, 1.5–3 Hz and 2–4 Hz), we observe changes of −0.0890%/-0.5935%, −0.6903%/-4.7754% and −1.1751%/-7.0358% for a 10% and 40% Vs velocity decrease, respectively. Expected associated changes in density and Vp have not been taken into account here.

Using the 1D-velocity model, we also compute Rayleigh wave sensitivity kernels with the python library disba (Luu, 0000), for the different target frequencies (Fig. 9d). For all frequencies, there is high sensitivity close to the surface (below 40 m). These depth ranges are well aligned with the depth at which clay occurs in our study area, making this approach relevant for the potential detection of environmental and subsurface changes that could precede a quick clay-related

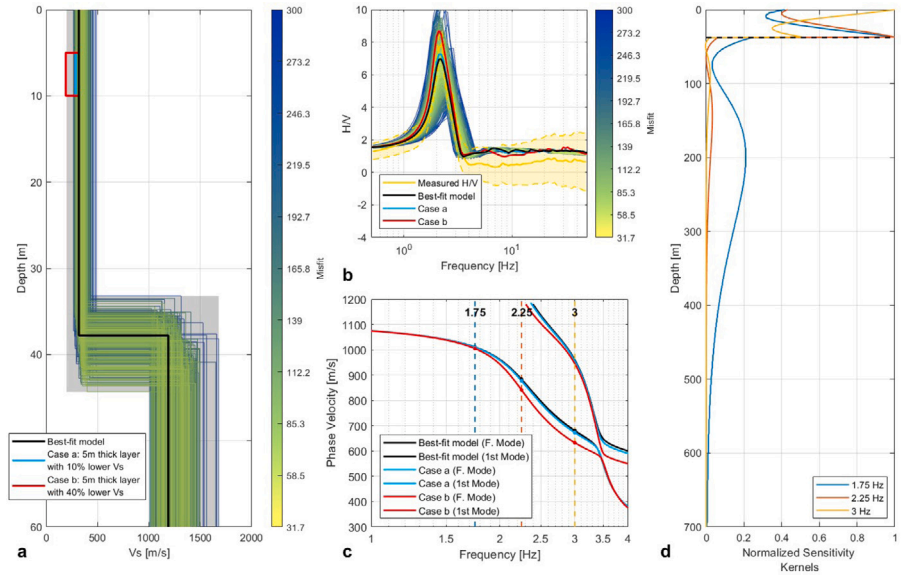

Fig. 9. Dispersion curves: (a) Vs profile with inverted model with misfit less than 100. (b) Horizontal to vertical spectral ratio. Measured H/V for the ALNN3 station are shown in yellow as mean and standard deviation. The best-fit inverted model is shown as black line and the two cases (Case a and Case b) corresponding to a reduction of 10% and 40% Vs velocity as red and blue lines, respectively. (c) Theoretical dispersion curves for the ALNN3 station showing the fundamental and first mode. (d) Rayleigh wave sensitivity kernels for the different target frequencies in the depth 0–700 m. (For interpretation of the references to color in this figure legend, the reader is referred to the web version of this article.)

landslide. This also supports the high sensitivity to freezing in the uppermost part of the subsurface in all frequency bands. Furthermore, the different depths of the bedrock at the two analyzed sites at Alna are probably captured to some extent by all frequency ranges.

7. Discussion of the potential for quick clay failure monitoring

In this study, our aim is to obtain information on the feasibility of using low-cost seismic sensors for quick clay failure monitoring systems in urban quick clay areas, by analyzing the seismic velocity variation (dv/v) derived from urban seismic noise. First, we have investigated the variability of the noise field (see Section 3). The temporal resolution of velocity variations is limited by changes in the noise field, i.e., strong day-night and week-weekend variation. Despite the significant variability in the noise field, mostly due to variations associated with the urban rhythm of life, we are able to obtain stable noise correlation functions for 1-day stacks. The week-weekend fluctuations due to human activity are visible in our dv/v results; however, these changes are smaller than the changes associated with subsurface changes and lie within the dv/v measurement error. However, these urban noise variations could mask the smaller dv/v variations, and therefore we recommend a careful analysis of all dv/v patterns including different components and their average in different frequency bands.

Second, we investigated the extracted velocity changes and interpreted spatio-temporal variations with respect to environmental measurements. The dv/v results obtained in our study are mainly due to shallow changes in the subsurface, being dominated by environmental effects. Environmental factors, such as freezing and thawing, were found to produce large velocity variations, as similarly observed by Gassenmeier et al. (2014), Steinmann et al. (2021). During winter months, freezing and thawing dominate velocity variations and could therefore mask potential changes related to other subsurface processes (Gassenmeier et al., 2014). However, it may give us other insight into the effect of freezing and thawing on the ground properties. The process of freezing and thawing cycles significantly affects the mechanical and hydraulic properties of clay soils. Repeated freeze-thaw cycles alter soil structure, affecting its strength, cohesion, and hydraulic conductivity. For example, in terms of hydraulic properties, Benson and Othman (1993) have explored the behavior of compacted clay specimens in both laboratory and field under freeze-thaw conditions. They observed that the overall hydraulic conductivity remained largely unchanged. However, redistribution and desiccation of water, mostly above but also just below the freezing plane caused a localized increases in hydraulic conductivity. In terms of mechanical property, Wang et al. (2018) conducted a laboratory experiment and revealed that with an increasing number of freeze-thaw cycles, the static strength and cohesion of the clay decreased exponentially, indicating a deterioration in the soil structure. However, they also observed an exponential increase of the friction coefficient. This suggests that while the soil becomes weaker overall, it might resist more to sliding. Observations of freezing and thawing cycles via dv/v as we show here therefore has the potential to better understand these processes.

Our results also reveal changes in pore pressure/water level in the subsurface. In contrast to borehole point measurements, seismic methods have the advantage that they are sensitive to a larger area, and we can use different frequencies to probe different depths and give a more complete picture of the subsurface. It is also non-invasive. These measurements can therefore complement the pore pressure measurements, for example those made during the construction of the new water supply tunnels in Oslo.

We also observe a hysteresis between the dv/v and the pore pressure which can be used to visualize the soil behavior under changes in moisture condition. An increase in the distance between the wetting and drying curves is indicative of a change in soil behavior, linked to its ability to retain and drain water derived from precipitation or snowmelt. This change can lead to higher pore pressures, reduced soil strength, and ultimately, slope failure (e.g. Yang et al. (2019), Han et al. (2021)). Thus, the hysteresis effect can also provide insight into potential landslide hazard. By understanding how the soil's ability to retain and release water changes over time, hysteresis analysis can help to predict critical shifts in pore pressure and mechanical stability, improving monitoring systems and mitigation strategies for landslides.

In order to monitor and alert on quick clay instability, we need: i) more or less constant dv/v when the quick clay is stable, meaning stable noise sources as well as limited environmental influences, and (ii) that the frequencies that we are using are sensitive at the depth where the quick clay could destabilize, so that a reduction in rigidity would be visible in the dv/v.

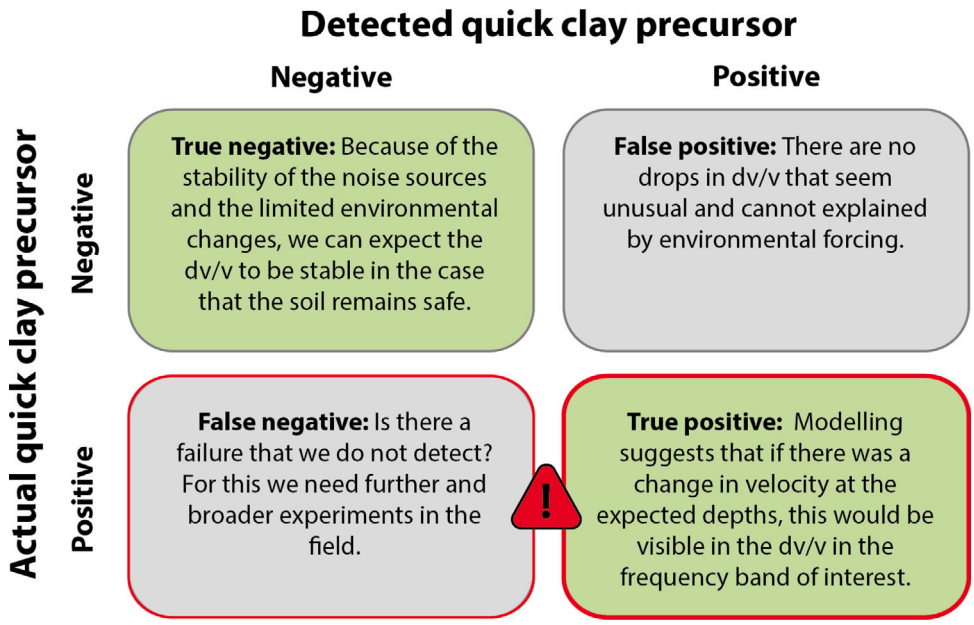

Fig. 10. Summary of possible outcomes from failure quick clay precursor monitoring.

We summarize the different possible outcomes for failure precursor monitoring in Fig. 10. Can we expect the dv/v to not vary when there is no change in quick clay stability? In the case of stability of the noise sources and limited environmental changes, which could potentially be modeled and removed, we can indeed expect the dv/v to remain stable in the case that the soil remains stable.

Do we observe any unusual changes in dv/v when the soil remains stable, i.e, can we avoid false alarms? During the time that we investigated, there are no drops in dv/v that seem unusual, except for the extreme weather event Hans. However, the fact that the drops in dv/v associated with Hans correlates well with pore pressure measurements and water levels and it is limited in time, well explains that it is caused by environmental forcing and would allow modeling and removing the change from the dv/v time series.

Would we detect a quick clay failure precursor if there is one? For quick clay, we do not know what to expect: the change might be larger than the -7% drop observed by Mainsant et al. (2012) several days before a clay landslide, but also the time lag between this change and the slide might be very short. Since we did not observe/record during a quick clay failure in this study, we cannot define a precursor. However, theoretical dispersion curves (Fig. 9c) indicate that the frequencies used in our study are sensitive to a velocity change at the depths where we expect the quick clay to destabilize, indicating the potential for detecting such changes.

Lastly, could there be a failure that we are not able to detect in the dv/v, i.e., a false negative? For answering this we need further and broader experiments. However, there could of course occur dv/v variations due to environmental forcing, such as freezing and thawing effects, that could mask a small medium change related to quick clay failure.

8. Conclusion

In summary, our study gave us insights into what kind of subsurface changes can be resolved and are expected over longer time periods and under stable conditions in the quick clay area under investigation in Oslo. This will potentially allow us to identify unusual or permanent changes that cannot be explained by the environmental parameters investigated in this study. This builds a baseline for a quick clay failure monitoring system, and demonstrates the importance and opportunity to conduct further tests and experiments in the field. The computed dispersion curves allowed us to verify the sensitivity of surface waves in the frequency band of interest to velocity change at depth. Therefore, observed velocity variations at the site has potential for monitoring quick clay instabilities.

CRediT authorship contribution statement

Charlotte Bruland: Writing – original draft, Visualization, Methodology, Formal analysis, Conceptualization. **Anna Maria Dichiarante:** Writing – review & editing, Visualization, Methodology, Formal analysis, Conceptualization. **Andreas Köhler:** Writing – review & editing, Visualization, Methodology, Investigation, Data curation, Conceptualization. **Volker Oye:** Supervision, Investigation, Conceptualization. **Ivan Van Bever:** Writing – review & editing. **Eric Larose:** Writing – review & editing, Methodology.

Acknowledgments

We acknowledge the Norwegian Research Council for their support through the GEObyIT project (grant no. 311596) and Centre for Geophysical Forecasting (project no. 309960). We also acknowledge the Oslo municipality and Ingjerd Mørck for providing pore pressure measurements and valuable discussions. We are grateful to Valerie Maupin and Marouchka Froment for helpful discussions on sensitivity kernels. We thank the editor and reviewers for their comments, which helped improve the manuscript.

Declaration of competing interest

The authors declare that they have no known competing financial interests or personal relationships that could have appeared to influence the work reported in this paper.

Appendix A. Supplementary data

Supplementary material related to this article can be found online at https://doi.org/10.1016/j.enggeo.2025.107936.

Data availability

Seismic data from the Oslo network until September 2023 are openly available at the Norwegian EIDA node Ottemöller et al. (2021) with the network code 4X Köhler (2021) (https://www.fdsn.org/networks/detail/4X_2021/). Weather data is obtained from The Norwegian Meteorological Institute (https://frost.met.no/index.html). Information about the water level in the Alna river is available through The Norwegian Water Resources and Energy Directorate (NVE) (https://sildre.nve.no/).

The analysis was done using the Obspy (Krischer et al., 2015), Numpy (Harris et al., 2020) and SciPy (Virtanen et al., 2020) libraries. Seismic (Makus and Sens-Schönfelder, 2023) was used for computing auto-correlations and single station cross-correlations and measuring relative velocity changes. Geopsy (Wathelet et al., 2020) and HVInv (García-Jerez et al., 2016) where used in the H/V inversion and dispersion curves. For computing Rayleigh wave sensitivity kernels we used disba Luu (0000). Figures were created using Matplotlib (Hunter, 2007).

References

Albaric, J., Kühn, D., Ohrnberger, M., Langet, N., Harris, D., Polom, U., Lecomte, I., Hillers, G., 2021. Seismic monitoring of permafrost in Svalbard, Arctic Norway. Seism. Soc. Am. 92 (5), 2891–2904.

Arosio, D., Aguzzoli, A., Zanzi, L., Panzeri, L., Scaccabarozzi, D., 2023. Lab and field tests of a low-cost 3-component seismometer for shallow passive seismic applications. Earth Space Sci. 10 (10), e2023EA002934.

Benson, C.H., Othman, M.A., 1993. Hydraulic conductivity of compacted clay frozen and thawed in situ. J. Geotech. Eng. 119 (2), 276–294.

Bontemps, N., Lacroix, P., Larose, E., Jara, J., Taipe, E., 2020. Rain and small earthquakes maintain a slow-moving landslide in a persistent critical state. Nat. Commun. 11 (1), 780.

Bottelin, P., Baillet, L., 2024. Original insights into rock slope damage processes until collapse from passive seismic monitoring. Geophys. Res. Lett. 51 (13), e2024GL109139.

Brenguier, F., Shapiro, N.M., Campillo, M., Ferrazzini, V., Duputel, Z., Coutant, O., Nercessian, A., 2008. Towards forecasting volcanic eruptions using seismic noise. Nat. Geosci. 1 (2), 126–130.

Campillo, M., Paul, A., 2003. Long-range correlations in the diffuse seismic coda. Science 299 (5606), 547–549.

Chouet, B.A., Matoza, R.S., 2013. A multi-decadal view of seismic methods for detecting precursors of magma movement and eruption. J. Volcanol. Geotherm. Res. 252, 108–175.

Clements, T., Denolle, M.A., 2018. Tracking groundwater levels using the ambient seismic field. Geophys. Res. Lett. 45 (13), 6459–6465.

Denton, P., 2014. One step beyond. Astron. Geophys. 55 (5), 5–30.

Díaz, J., Ruiz, M., Sánchez-Pastor, P.S., Romero, P., 2017. Urban seismology: On the origin of earth vibrations within a city. Sci. Rep. 7 (1), 15296.

Duputel, Z., Ferrazzini, V., Brenguier, F., Shapiro, N., Campillo, M., Nercessian, A., 2009. Real time monitoring of relative velocity changes using ambient seismic noise at the Piton de la Fournaise volcano (La Réunion) from January 2006 to June 2007. J. Volcanol. Geotherm. Res. 184 (1–2), 164–173.

Erlingsson, S., Bodare, A., 1996. Live load induced vibrations in ullevi stadium—dynamic dynamic soil analysis. Soil Dyn. Earthq. Eng. 15 (3), 171–188.

Fokker, E., Ruigrok, E., Hawkins, R., Trampert, J., 2021. Physics-based relationship for pore pressure and vertical stress monitoring using seismic velocity variations. Remote. Sens. 13 (14), 2684.

Fokker, E., Ruigrok, E., Hawkins, R., Trampert, J., 2023. 4D physics-based pore pressure monitoring using passive image interferometry. Geophys. Res. Lett. 50 (5), e2022GL101254.

Fuchs, F., Bokelmann, G., Group, A.W., 2018. Equidistant spectral lines in train vibrations. Seismol. Res. Lett. 89 (1), 56–66.

Garambois, S., Voisin, C., Romero Guzman, M., Brito, D., Guillier, B., Réfloch, A., 2019. Analysis of ballistic waves in seismic noise monitoring of water table variations in a water field site: added value from numerical modelling to data understanding. Geophys. J. Int. 219 (3), 1636–1647.

García-Jerez, A., Piña-Flores, J., Sánchez-Sesma, F.J., Luzón, F., Perton, M., 2016. A computer code for forward calculation and inversion of the H/V spectral ratio under the diffuse field assumption. Comput. Geosci. 97, 67–78.

Gassenmeier, M., Sens-Schönfelder, C., Delatre, M., Korn, M., 2014. Monitoring of environmental influences on seismic velocity at the geological storage site for CO2 in Ketzin (Germany) with ambient seismic noise. Geophys. J. Int. 200 (1), 524–533.

Gaubert-Bastide, T., Garambois, S., Bordes, C., Voisin, C., Oxarango, L., Brito, D., Roux, P., 2022. High-resolution monitoring of controlled water table variations from dense seismic-noise acquisitions. Water Resour. Res. 58 (8), e2021WR030680.

Ghione, F., Köhler, A., Dichiarante, A.M., Aarnes, I., Oye, V., 2023. Vs30 and depth to bedrock estimates from integrating HVSR measurements and geology-slope approach in the Oslo area, Norway. Front. Earth Sci. 11, 1242679.

Groos, J., Ritter, J., 2009. Time domain classification and quantification of seismic noise in an urban environment. Geophys. J. Int. 179 (2), 1213–1231.

Hadziioannou, C., Larose, E., Coutant, O., Roux, P., Campillo, M., 2009. Stability of monitoring weak changes in multiply scattering media with ambient noise correlation: Laboratory experiments. J. Acoust. Soc. Am. 125 (6), 3688–3695.

Han, H., Shi, B., Zhang, L., 2021. Prediction of landslide sharp increase displacement by SVM with considering hysteresis of groundwater change. Eng. Geol. 280, 105876.

Harris, C.R., Millman, K.J., Van Der Walt, S.J., Gommers, R., Virtanen, P., Cournapeau, D., Wieser, E., Taylor, J., Berg, S., Smith, N.J., et al., 2020. Array programming with numpy. Nature 585 (7825), 357–362.

Healy, D., 2023. Listening to Manchester: Using citizen science Raspberry Shake seismometers to quantify road traffic.

Hinzen, K.-G., Krummel, H., Weber, B., Fleischer, C., 2022. Forensic view on two raspberry shake burglargrams. J. Seism. 26 (5), 863–873.

Holmgren, J.M., Werner, M.J., 2021. Raspberry shake instruments provide initial ground-motion assessment of the induced seismicity at the united downs deep geothermal power project in Cornwall, United Kingdom. Seism. Rec. 1 (1), 27–34.

Hunter, J.D., 2007. Matplotlib: A 2D graphics environment. Comput. Sci. Eng. 9 (03), 90–95.

Illien, L., Sens-Schönfelder, C., Ke, K.-Y., 2023. Resolving minute temporal seismic velocity changes induced by earthquake damage: the more stations, the merrier? Geophys. J. Int. 234 (1), 124–135.

James, S., Knox, H., Abbott, R., Panning, M., Screaton, E., 2019. Insights into permafrost and seasonal active-layer dynamics from ambient seismic noise monitoring. J. Geophys. Res.: Earth Surf. 124 (7), 1798–1816.

Jerkins, A.E., Oye, V., Alvizuri, C., Halpaap, F., Kværna, T., 2024. The 21 March 2022 M w 5.1 Tampen Spur Earthquake, North Sea: Location, Moment Tensor, and context. Bull. Seismol. Soc. Am. 114 (2), 741–757.

Khaldoun, A., Moller, P., Fall, A., Wegdam, G., de Leeuw, B., Méheust, Y., et al., 2004. Quick clay and landslides of clayey soils. Phys. Rev. Lett. 103.

Köhler, A., 2021. Geobyit seismic network in Oslo, Norway. http://dx.doi.org/10.7914/3DMS-SJ84, URL https://www.fdsn.org/networks/detail/4X_2021/.

Köhler, A., Myklebust, E., Dichiarante, A.M., Oye, V., 2024. Monitoring urban construction and quarry blasts with low-cost seismic sensors and deep learning tools in the city of Oslo, Norway. Seismica 3 (1).

Krischer, L., Megies, T., Barsch, R., Beyreuther, M., Lecocq, T., Caudron, C., Wassermann, J., 2015. ObsPy: A bridge for seismology into the scientific python ecosystem. Comput. Sci. Discov. 8 (1), 014003.

Larose, E., Carrière, S., Voisin, C., Bottelin, P., Baillet, L., Guéguen, P., Walter, F., Jongmans, D., Guillier, B., Garambois, S., et al., 2015. Environmental seismology: What can we learn on earth surface processes with ambient noise? J. Appl. Geophys. 116, 62–74.

Lavoué, F., Coutant, O., Boué, P., Pinzon-Rincon, L., Brenguier, F., Brossier, R., Dales, P., Rezaeifar, M., Bean, C.J., 2021. Understanding seismic waves generated by train traffic via modeling: Implications for seismic imaging and monitoring. Seism. Soc. Am. 92 (1), 287–300.

Le Breton, M., Bontemps, N., Guillemot, A., Baillet, L., Larose, É., 2021. Landslide monitoring using seismic ambient noise correlation: challenges and applications. Earth-Sci. Rev. 216, 103518.

Lecocq, T., Hicks, S.P., Van Noten, K., Van Wijk, K., Koelemeijer, P., De Plaen, R.S., Massin, F., Hillers, G., Anthony, R.E., Apoloner, M.-T., et al., 2020. Global quieting of high-frequency seismic noise due to COVID-19 pandemic lockdown measures. Science 369 (6509), 1338–1343.

Lecocq, T., Longuevergne, L., Pedersen, H.A., Brenguier, F., Stammler, K., 2017. Monitoring ground water storage at mesoscale using seismic noise: 30 years of continuous observation and thermo-elastic and hydrological modeling. Sci. Rep. 7 (1), 14241.

Lindner, F., Wassermann, J., Igel, H., 2021. Seasonal freeze-thaw cycles and permafrost degradation on Mt. Zugspitze (German/Austrian Alps) revealed by single-station seismic monitoring. Geophys. Res. Lett. 48 (18), e2021GL094659.

Lobkis, O.I., Weaver, R.L., 2001. On the emergence of the Green's function in the correlations of a diffuse field. J. Acoust. Soc. Am. 110 (6), 3011–3017.

Luu, K., 0000. disba: Numba-accelerated computation of surface wave dispersion, URL https://github.com/keurfonluu/disba, http://dx.doi.org/10.5281/zenodo.3987395.

Maciel, S.T.R., Rocha, M.P., Schimmel, M., 2021. Urban seismic monitoring in Brasília, Brazil. Plos One 16 (8), e0253610.

Mainsant, G., Larose, E., Brönnimann, C., Jongmans, D., Michoud, C., Jaboyedoff, M., 2012. Ambient seismic noise monitoring of a clay landslide: Toward failure prediction. J. Geophys. Res.: Earth Surf. 117 (F1).

Makus, P., Sens-Schönfelder, C., 2023. SeisMIC-an open source python toolset to compute velocity changes from ambient seismic noise.

Makus, P., Sens-Schönfelder, C., Illien, L., Walter, T.R., Yates, A., Tilmann, F., 2023. Deciphering the whisper of volcanoes: Monitoring velocity changes at Kamchatka's Klyuchevskoy group with fluctuating noise fields. J. Geophys. Res.: Solid Earth 128 (4), e2022JB025738.

Masterlark, T., Haney, M., Dickinson, H., Fournier, T., Searcy, C., 2010. Rheologic and structural controls on the deformation of Okmok volcano, Alaska: FEMs, inSAR, and ambient noise tomography. J. Geophys. Res.: Solid Earth 115 (B2).

McNamara, D.E., Buland, R.P., 2004. Ambient noise levels in the continental United States. Bull. Seismol. Soc. Am. 94 (4), 1517–1527.

Mikesell, T.D., Malcolm, A.E., Yang, D., Haney, M.M., 2015. A comparison of methods to estimate seismic phase delays: Numerical examples for coda wave interferometry. Geophys. J. Int. 202 (1), 347–360.

Milana, G., Cultrera, G., Bordoni, P., Bucci, A., Cara, F., Cogliano, R., Di Giulio, G., Di Naccio, D., Famiani, D., Fodarella, A., et al., 2020. Local site effects estimation at Amatrice (Central Italy) through seismological methods. Bull. Earthq. Eng. 18, 5713–5739.

Obermann, A., Planès, T., Hadziioannou, C., Campillo, M., 2016. Lapse-time-dependent coda-wave depth sensitivity to local velocity perturbations in 3-D heterogeneous elastic media. Geophys. J. Int. 207 (1), 59–66.

Obermann, A., Planès, T., Larose, E., Sens-Schönfelder, C., Campillo, M., 2013. Depth sensitivity of seismic coda waves to velocity perturbations in an elastic heterogeneous medium. Geophys. J. Int. 194 (1), 372–382.

Okamoto, T., Larsen, J.O., Matsuura, S., Asano, S., Takeuchi, Y., Grande, L., 2004. Displacement properties of landslide masses at the initiation of failure in quick clay deposits and the effects of meteorological and hydrological factors. Eng. Geol. 72 (3–4), 233–251.

Ottemöller, L., Michalek, J., Christensen, J.-M., Baadshaug, U., Halpaap, F., Natvik, Ø., Kvæ rna, T., Oye, V., 2021. UiB-NORSAR EIDA node: Integration of seismological data in Norway. Seism. Soc. Am. 92 (3), 1491–1500.

Peterson, J., et al., 1993. Observations and Modeling of Seismic Background Noise, vol. 93, US Geological Survey Reston, VA, USA.

Riahi, N., Gerstoft, P., 2015. The seismic traffic footprint: Tracking trains, aircraft, and cars seismically. Geophys. Res. Lett. 42 (8), 2674–2681.

Rodríguez Tribaldos, V., Ajo-Franklin, J.B., 2021. Aquifer monitoring using ambient seismic noise recorded with distributed acoustic sensing (DAS) deployed on dark fiber. J. Geophys. Res.: Solid Earth 126 (4), e2020JB021004.

Rørstadbotnen, R.A., Dong, H., Landrø, M., Duffaut, K., Growe, K., Kakhkhorov, U., Wienecke, S., Jacobsen, J., 2023. Quick clay monitoring using distributed acoustic sensing: A case study from Rissa, Norway. Geophysics 88 (5), B267–B283.

Salvermoser, J., Hadziioannou, C., Stähler, S.C., 2015. Structural monitoring of a highway bridge using passive noise recordings from street traffic. J. Acoust. Soc. Am. 138 (6), 3864–3872.

Sánchez-Pastor, P., Obermann, A., Schimmel, M., Weemstra, C., Verdel, A., Jousset, P., 2019. Short-and long-term variations in the Reykjanes geothermal reservoir from seismic noise interferometry. Geophys. Res. Lett. 46 (11), 5788–5798.

Schimmel, M., Stutzmann, E., Gallart, J., 2011. Using instantaneous phase coherence for signal extraction from ambient noise data at a local to a global scale. Geophys. J. Int. 184 (1), 494–506.

Sens-Schönfelder, C., Wegler, U., 2006. Passive image interferometry and seasonal variations of seismic velocities at Merapi Volcano, Indonesia. Geophys. Res. Lett. 33 (21).

Snieder, R., Grêt, A., Douma, H., Scales, J., 2002. Coda wave interferometry for estimating nonlinear behavior in seismic velocity. Science 295 (5563), 2253–2255.

Steinmann, R., Hadziioannou, C., Larose, E., 2021. Effect of centimetric freezing of the near subsurface on Rayleigh and Love wave velocity in ambient seismic noise correlations. Geophys. J. Int. 224 (1), 626–636.

Tepp, G., Stubailo, I., Kohler, M., Guy, R., Bozorgnia, Y., 2024. Shake to the beat: Exploring the seismic signals and stadium response of concerts and music fans. Authorea Preprints.

Tomás, R., Abellán, A., Cano, M., Riquelme, A., Tenza-Abril, A., Baeza-Brotons, F., Saval, J., Jaboyedoff, M., 2018. A multidisciplinary approach for the investigation of a rock spreading on an urban slope. Landslides 15, 199–217.

Virtanen, P., Gommers, R., Oliphant, T.E., Haberland, M., Reddy, T., Cournapeau, D., Burovski, E., Peterson, P., Weckesser, W., Bright, J., et al., 2020. Scipy 1.0: fundamental algorithms for scientific computing in python. Nature Methods 17 (3), 261–272.

Voisin, C., Garambois, S., Massey, C., Brossier, R., 2016. Seismic noise monitoring of the water table in a deep-seated, slow-moving landslide. Interpretation 4 (3), SJ67–SJ76.

Voisin, C., Guzmán, M.A.R., Réfloch, A., Taruselli, M., Garambois, S., 2017. Groundwater monitoring with passive seismic interferometry. J. Water Resour. Prot. 9 (12), 1414–1427.

Wang, Q.-Y., Brenguier, F., Campillo, M., Lecointre, A., Takeda, T., Aoki, Y., 2017. Seasonal crustal seismic velocity changes throughout Japan. J. Geophys. Res.: Solid Earth 122 (10), 7987–8002.

Wang, M., Meng, S., Sun, Y., Fu, H., 2018. Shear strength of frozen clay under freezing-thawing cycles using triaxial tests. Earthq. Eng. Eng. Vib. 17, 761–769.

Wathelet, M., Chatelain, J.-L., Cornou, C., Giulio, G.D., Guillier, B., Ohrnberger, M., Savvaidis, A., 2020. Geopsy: A user-friendly open-source tool set for ambient vibration processing. Seismol. Res. Lett. 91 (3), 1878–1889.

Weaver, R.L., Hadziioannou, C., Larose, E., Campillo, M., 2011. On the precision of noise correlation interferometry. Geophys. J. Int. 185 (3), 1384–1392.

Yang, Z., Cai, H., Shao, W., Huang, D., Uchimura, T., Lei, X., Tian, H., Qiao, J., 2019. Clarifying the hydrological mechanisms and thresholds for rainfall-induced landslide: in situ monitoring of big data to unsaturated slope stability analysis. Bull. Eng. Geol. Environ. 78, 2139–2150.